PARAMETER ANALYSIS AND OPTIMIZATION OF A HEAT SINK FOR COOLING INTELLIGENT POWER MODULES BASED ON TAGUCHI METHOD

by

Wenhao DING, Peng YANG*, Pengfan CHEN, and Yingwen LIU*

Key Laboratory of Thermo-Fluid Science and Engineering of MOE,
School of Energy and Power Engineering, Xi'an Jiaotong University, Xi'an, Shaanxi, China

Original scientific paper
https://doi.org/10.2298/TSCI221107070D

The stability of the intelligent power module has a very significant impact on the operation of the air conditioner. In this paper, a prototype experimental platform is built to verify the feasibility of the simulation results. Next, the thermal performance and flow characteristics of the heat sink are analyzed, including single-factor analysis and analysis of interactive effects. The results show that a smaller pipe diameter can reduce the maximum temperature of intelligent power modules, T_{IPM}, but it will increase the pressure drop, ΔP, and entropy generation. The thickness of the heat sink plate and the height of the protruding table have an interactive effect on the T_{IPM}. Then the sensitivity of the T_{IPM} and pressure drop to different parameters was analyzed, and the contribution ratio of the pipe diameter to both the T_{IPM} and pressure drop was the largest. Finally, the optimal combination of parameters was obtained to minimize both the T_{IPM} and pressure drop. Compared with the original structure, the T_{IPM} decreased by 3.98 K.

Key words: *liquid cooling, intelligent power module, heat sink, sensitivity analysis, Taguchi method*

Introduction

Intelligent power module (IPM) is the key component of the inverter air conditioner. The reliability of IPM design directly affects the reliability of inverter air conditioners. Due to the high level of integration, the heat generated by IPM is considerable [1, 2]. Working at a higher temperature for a long time will greatly shorten the service life of IPM [3]. So, reasonable control of the temperature rise can greatly improve the service life and reliability of IPM.

Generally, the heat dissipation methods of electronic components include air cooling and liquid cooling. Yuan *et al.* [4] applied the plate needle fin radiator to the cooling of a desktop PC CPU at a heat flux of 2.20 W/cm^2. The results show that the temperature can be kept below 358 K. Han *et al.* [5] evaluated the radiator's thermal performance based on the fins' shape. The results show that the radiator with perforated fins has good thermal performance.

Although the air-cooled heat sink is simple in structure and easy to maintain, its convective heat transfer coefficient is not high and its cooling capacity is limited [6]. The heat transfer coefficient of a liquid cooling system is several orders of magnitude higher than that of air cooling systems. Liu *et al*. [7] compared the thermal performance of insulated gate bipolar transistor (IGBT) power modules with direct liquid cooling and indirect liquid cooling. The re-

* Corresponding authors, e-mail: yp2019@mail.xjtu.edu.cn, ywliu@xjtu.edu.cn

sults show that the thermal resistance of the direct liquid-cooled IGBT power module is reduced by 25%. Seokkan *et al*. [8] developed a liquid cooling module inspired by the human respiratory system. While providing a high cooling capacity, the cooling module shows very low thermal resistance and pressure drop. Lu *et al*. [9] developed a new type of heat pipe radiator with a parallel heat flow structure. Compared to typical heat pipe radiators, the new radiator offers a 25% reduction in thermal resistance. Pan *et al.* [10] designed and studied a micro-channel liquid cooling heat sink integrated vapor chamber (VC integrated heat sink). The results show that the VC integrated heat sink has a lower thermal resistance and better temperature uniformity. Natarajan *et al*. [11] designed and fabricated a liquid microjet array device using multi-layer ceramic technology. It has the ability to be larger than 2.5 MW/m^2, and the pressure drop is less than 70 kPa. Bhunia *et al*. [12] developed a closed-loop liquid jet impingement cooling technology. The research results show that this technology has a heat dissipation capacity of 1623 W, which is 1.8 times higher than that of the most advanced needle fin heat sink. Wang *et al*. [13] used the integrated liquid cooling technique to cooling IGBT modules in hybrid and electric vehicles to improve the operating life and reliability of these modules. Yang *et al*. [14] analyzed the effects of the number of pipes, pipe diameters and connection mode on the heat sink for cooling the IPM and applied the response surface method to optimize the structure of the heat sink, which resulted in a 4.55 K reduction in the maximum temperature of the IPM. Hu and Wei [15] performed finite element modelling (FEM) analysis of the IGBT heat sink, adopted aluminum alloy housing and AIN heat transfer module, and designed a double-sided heat dissipation scheme, which can significantly improve the heat dissipation effect. Cheng *et al*. [16] designed a new inverter cooling and waste heat recovery solution that not only keeps all electronic components within the normal temperature range, but also improves system energy efficiency by about 4%.The coolant in liquid cooling is not only water but also liquid metal [17-20] and refrigerant.

In previous work, the influence of structure parameters on cooling effect has been studied, but did not analyse the contribution of each parameter to the response value, which might cause misinterpretation of results. In addition, the traditional one-factor method requires a lot of experiments and is very time-consuming. Therefore, there is an urgent need for a practical and efficient method to carry out parametric analysis and optimization of an IPM heat sink in limited numerical experiments. The Taguchi method is founded by Gunes *et al*. [21]. Yu *et al*. [22] used Taguchi method to analyze and optimize a parallel shell-and-tube heat exchanger, and the comprehensive performance of the heat exchanger was improved by 0.19-1.92%. This method was used by Yakut *et al.* [23, 24] to investigate the effect of different design parameters on the thermal resistance and pressure drop characteristics of the hexagonal fin heat sink, to maximize the performance of the heat exchanger. Many scholars [25-28] have used the Taguchi method for heat exchanger-related studies and optimization and their results have shown that Taguchi method can be successfully and efficiently applied to heat transfer studies.

In this study, an experimental platform was built to verify the feasibility of the simulation results. A 3-D computational fluid dynamics model was established. The effects of the three parameters on the T_{IPM} and pressure drop were analyzed. Then, the sensitivity of the T_{IPM} and pressure drop to different parameters was analyzed. Finally, the optimal combination of parameters was obtained to minimize the T_{IPM} and pressure drop. This project mainly analyzes the structural parameters of the IPM heat sink, takes into account the influence of each parameter on the cooling effect, and uses the Taguchi method to analyse and obtain the optimal structure. This study provides theoretical guidance and data support for further improvement of the IPM heat sink.

Description of the experimental set-up and numerical simulation model

Experimental system

The schematic diagram of the refrigeration system is shown in fig. 1. After cooling in the condenser, part of the refrigerant is diverted to the heat sink to carry away the heat generated by the IPM and then passes through the throttle valve-2 and enters the evaporator. The experimental testing rig was built as shown in fig. 2. The system has two rooms, A and B. Room A is used to simulate the outdoor environment with a temperature of 326.15 K and Room B is an indoor environment. When the temperature in Room B is stable, the data measured by the *T*-type thermocouple is transmitted to the data collector and then to the computer for analysis. Copper-constantan *T*-type thermocouples were used to measure the temperature with an error of ±0.2 K. The measurement of the pressure drop was done through a differential pressure sensor (Rosemount 3051) with an error of 0.04%. The heat sink is shown in fig. 3. The substrate is made of aluminum and the material of the pipe is copper. Four electronic components are installed on the substrate: IPM, diode, IGBT, and rectifier bridge, with a total calorific value of about 110 W. The calorific value and size of the electronic components are shown in tab. 1. The electronic components is simulated through the power supply, and the heating power of the electronic components is controlled by adjusting the input voltage with an uncertainty of ±0.02 W.

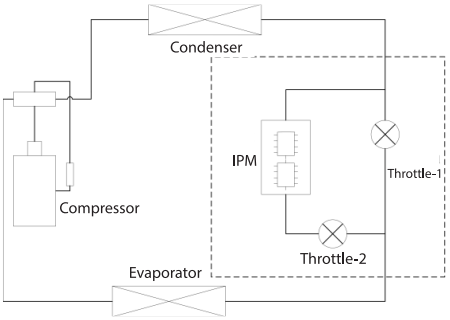

Figure 1. The schematic diagram of the refrigeration system

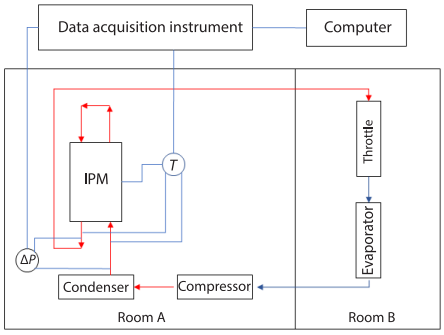

Figure 2. Schematic diagram of the experimental system

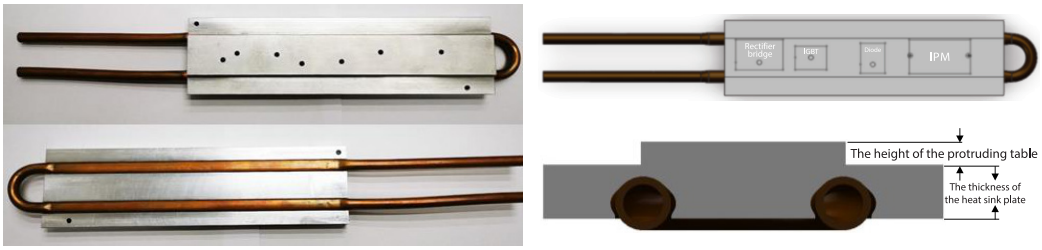

Figure 3. Physical diagram and 3-D model of the heat sink; (a) physical diagram and (b) 3-D model

Table 1. Calorific value and size of electronic componen

	Unit	IPM	IGBT	Diode	Rectifier bridge	Total
Heat generation	[W]	71.5	22.0	3.6	12.9	100
Size	[mm]	38.75 × 22.33	19.86 × 15.36	20 × 15.5	30 × 20	–

Numerical simulation

Geometry configuration of the heat sink

The dimension of the heat sink is 177 mm × 50 mm × 10 mm. Each of the four electronic components is assumed to be a surface heat source with constant heat flux. The simulation model was developed according to the following assumptions:

– The flow is steady and incompressible.
– The material properties are non-temperature dependent.
– The heat radiation between the heat sink and environment air is excluded.
– The contact thermal resistance is excluded.

Governing equations and boundary conditions

The governing equations employed in the present study include the conservation conservations of mass, momentum, and energy in their non-dimensional forms, which are given:

– Conservation of mass

$$\frac{\partial u_i}{\partial x_i} = 0 \tag{1}$$

– Conservation of momentum

$$\rho \frac{\partial}{\partial x_i}\left(u_i u_j\right) = -\frac{\partial P}{\partial x_j} + \mu \frac{\partial}{\partial x_i}\left(\frac{\partial u_j}{\partial x_i}\right) \tag{2}$$

– Conservation of energy

$$\rho c_p \frac{\partial}{\partial x_i}\left(u_i T\right) = \lambda \frac{\partial}{\partial x_i}\left(\frac{\partial T}{\partial x_i}\right) \tag{3}$$

The FLUENT was chosen for the heat sink's fluid dynamics and heat transfer simulation.The Reynolds number of R410A at the inlet is 23705, which indicates that the fluid is in a turbulent state. The realizable k-ε turbulence model is used. Table 2 lists the thermo-physical properties of R410A and boundary conditions.

Table 2. Thermo-physical properties of R410A and boundary conditions

Thermo-physical properties of R410A	Density [kgm^{-3}]	882.8
	Specific heat [Jkg^{-1}K^{-1}]	2418.7
	Thermal conductivity [WK^{-1}m^{-1}]	0.0731
	Viscosity [Pas]	$7.75 \cdot 10^{-5}$
Boundary conditions	Inlet mass-flow [kgs^{-1}]	$8.205 \cdot 10^{-3}$
	Inlet temperature [K]	327.65
	Pressure outlet [Pa]	0 (gauge pressure)
	Heat flux of IPM [Wm^{-2}]	81920
	Heat flux of diode [Wm^{-2}]	11899
	Heat flux of IGBT [Wm^{-2}]	70910
	Heat flux of rectifier bridge [Wm^{-2}]	21000
	Convection of outside wall [Wm^{-2}K]	8

Grid system and model validation

The ANSYS ICEM CFD was used to generate the tetrahedral grid as shown in fig. 4.

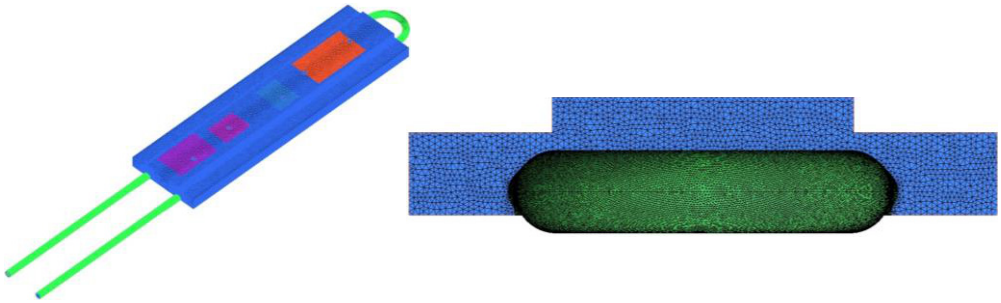

Figure 4. The FEM of the heat sink

For testing grid independence, the T_{IPM} and the pressure drop were compared with different grid sizes under the same boundary condition. As shown in tab. 3, the results indicate that the grid size of 5.0 million has shown a negligible difference between the T_{IPM} and the pressure drop as compared with a grid size of 16.0 million. That means the results based on 5.0 million cells are insensitive to further grid refinement, and the system is adopted for the numerical simulation model. As shown in tab. 4, the experimental and simulated values of the T_{IPM} were 350.21 K and 351.04 K, and the relative error is 0.24%. The experimental value of the outlet temperature was 332.54 K, while it was 332.92 K in the simulation, and the relative error is 0.11%. The good agreement shows that the numerical simulation is reliable for predicting the heat sink's performance.

Table 3. The simulation results of T_{IPM} and ΔP under different grid numbers

Grid numbers/million	1.0	2.5	5.0	8.0	16.0
T_{IPM} [K]	351.4	351.28	351.05	351.05	351.05
ΔP [Pa]	364.08	363.89	363.75	363.75	363.75

Table 4. Comparison of experimental and simulated values

	Maximum temperature [K]				Average temperature [K]	
	IPM	IGBT	Diode	Rectifier bridge	Inlet	Outlet
Experiment	350.21	345.34	339. 13	337.57	327.65	332.54
Simulation	351.04	345.91	339.25	337.85	327.65	332.92

Results and discussions

In this section, the effects of the pipe diameter, the thickness of the heat sink plate, and the height of the protruding table on the T_{IPM}, ΔP, and entropy generation, S_g, are studied. The T_{IPM} reflects the performance of the heat sink. The pressure drop is the pressure difference between the inlet and the outlet. Entropy generation [29] is calculated:

$$S_g = \dot{m}(s_1 - s_2) - S_f \tag{4}$$

where $\dot{m}$ is mass-flow, s_1 and s_2 are inlet and outlet specific entropy, s_f is the entropy change, and $S_f = Q/T_f - Q/T_{IPM}$, where Q is heat transfer capacity, and T_f – the temperature of R410A.

Effect of the pipe diameter

The thickness of the heat sink plate is set to 7 mm, the height of the protruding table is set to 3 mm, and the pipe diameter is 4-8 mm. The T_{IPM}, ΔP, and S_g are calculated as shown in fig. 5. The T_{IPM}, increases with the increase of pipe diameter. The change in pipe diameter has two main effects, on the one hand, with the increase in pipe diameter, the coupling area between the pipe and heat sink is larger, which means that the larger the heat transfer area is, on the other hand, when the mass-flow rate at the inlet is kept constant, with the increase of the pipe diameter, the velocity of the R410A decreases gradually, the Reynolds number decreases, and the convective heat transfer coefficient decreases, which plays an obstructive role in heat transfer. Therefore, under the comprehensive influence of the pipe diameter on heat transfer area and flow velocity, the increase of pipe diameter plays an obstructive role in the heat transfer, which is shown in that the T_{IPM}, increases with the increase of pipe diameter. Figure 6 shows the temperature distribution with different pipe diameters.

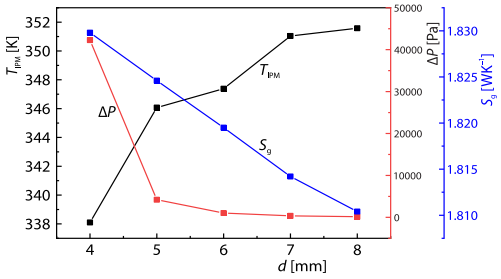

Figure 5. The T_{IPM}, ΔP, and S_g with different pipe diameters

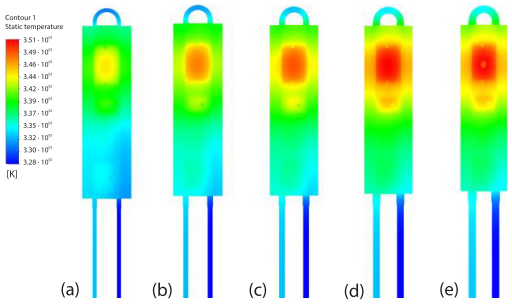

Figure 6. Temperature distribution with different pipe diameters; (a) d = 4 mm (b) d = 5 mm (c) d = 6 mm (d) d = 7 mm, and (e) d = 8 mm

When the pipe diameter increases, the pressure drop decreases. The flow velocity decreases, the resistance along the way and the local resistance decrease. However, the effect of pipe diameter on pressure drop decreases gradually with the increase of pipe diameter, especially when the pipe diameter increases above 7 mm or more. The total flow rate of the pipe-line is constant, with the increase of the pipe diameter, the cross-sectional area increases, the velocity decreases and the Reynold number decreases. The decrease in Nusselt number on the one hand leads to a decrease in the convective heat transfer coefficient, resulting in a decrease in the heat exchange, which in turn leads to a decrease in irreversible losses. The entropy production caused by heat transfer decreases. On the other hand, with the decrease of the inlet Reynold number of the fluid, the fluid is subjected to less friction during the flow process, so the entropy production due to fluid friction is also reduced. Therefore, the S_g decreases as the pipe diameter increases. When the pipe diameter increases, the pressure drop decreases and the irreversible loss in the heat transfer process decreases, which makes the S_g decrease gradually.

Effect of the thickness of the heat sink plate and the height of the protruding table

Effect of the thickness of the heat sink plate

The pipe diameter and the height of the protruding table are kept at 7 mm and 3 mm, respectively, and the thickness of the heat sink plate is chosen to be 6-10 mm. The T_{IPM} and S_g are calculated as shown in fig. 7. With the increase in the thickness of the heat sink plate, the

T_{IPM} decreases at first and then increases. Figure 8 shows the temperature distribution at different heat sink plate thicknesses. With the increase of the heat sink plate thickness, the T_{IPM} and high temperature areas first decrease and then increase. The pipe diameter remains constant, and the change in the thickness of the heat sink plate has very little effect on the flow state of refrigerant in the pipe, so the pressure drop and Nusselt number are unchanged. According to eq. (2), the entropy generation in the heat transfer process increases at first and then decreases.

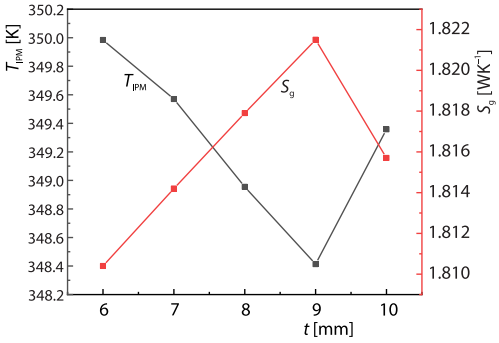

Figure 7. The T_{IPM} and S_g with different thicknesses

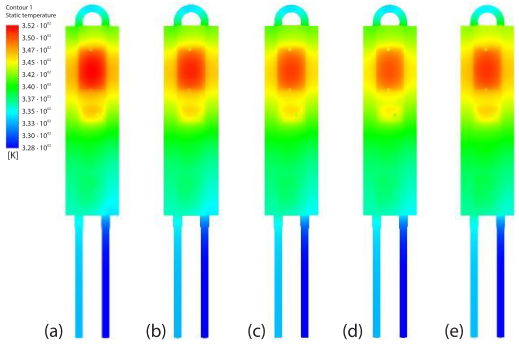

Figure 8. Temperature distribution with different thicknesses; (a) t = 6 mm, (b) t = 7 mm, (c) t = 8 mm, (d) t = 9 mm, and (e) t = 10 mm

In the numerical model of this study, the heat source is simplified to a surface, and the cold end is the fluid in the copper tube. According to the heat transfer path analysis, the heat is generated from the heat source, passes through the heat sink plate and the pipe employing heat conduction, and then is carried away by the refrigerant in the form of convective heat transfer. The heat does not go straight from the heat source to the cold end but reaches the refrigerant side from different directions. This means that the change of the thickness of the heat sink plate will increase or decrease the thermal resistance under a certain height of the protruding table and pipe diameter. Because the protruding table has a certain height, the heat does not reach the outer wall surface of the copper tube in a straight line. When the thickness of the heat sink is large, the heat is able to travel in a straight line from the heat source to the cold end, but the total heat transfer path becomes longer. When the thickness of the heat sink plate is very small, most of the heat is transferred to the part of the pipe near the middle of the heat sink, and it is difficult to transfer to the outer part of the pipe, thus increasing the total thermal resistance. As a result, the T_{IPM} increases while the thickness of the heat sink plate decreases. When the thickness of the heat sink plate is relatively large, although the heat can reach the pipe directly from IPM, the overall transfer path is still longer, so the T_{IPM} becomes larger.

Effect of the height of the protruding table

The pipe diameter and the thickness of the heat sink plate are set to 7 mm and 7 mm, respectively, and the height of the protruding table is 0 mm and 2-5 mm. The T_{IPM} and S_g are shown in fig. 9.

As shown in fig. 9, the T_{IPM} gradually decreases when the height of the protruding table is gradually increased. Consistent with the analysis in the previous section, when the height of the protruding table increases in a certain range, the total distance of heat from the hot source to the cold source decreases, so the T_{IPM} decreases. The entropy generation in the heat transfer process also increases with the height of the protruding table. Figure 10 shows temperature

distribution with different h. With the increase of h, the T_{IPM} and the high temperature area of the heat sink gradually decrease. Again, the change in the height of the protruding table has almost no effect on the flow state of the refrigerant in the pipe, so there is essentially no change in pressure drop when the height of the protruding table changes.

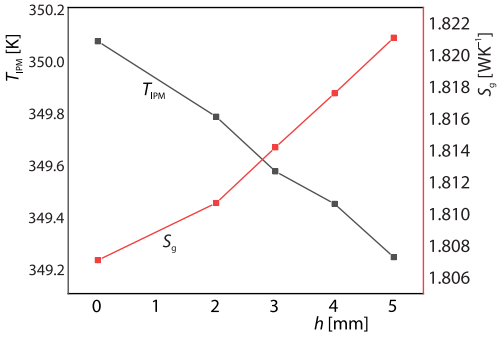

Figure 9. The T_{IPM} and entropy generation at different heights of the protruding table

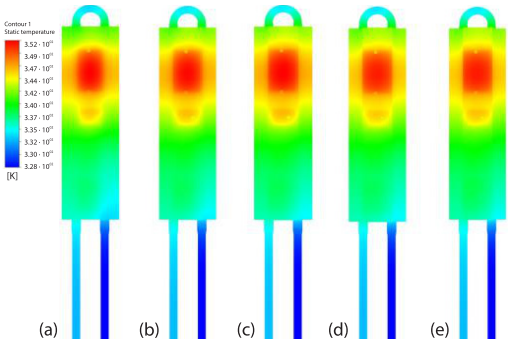

Figure 10. Temperature distribution with different thicknesses; (a) h = 0 mm, (b), h = 2 mm, (c) h = 3 mm, (d) h = 4 mm, and (e) h = 5 mm

Interaction effects of the thickness of the height of the protruding table

Keeping the pipe diameter at 7 mm and the sum of t and h at 10 mm, five combinations of parameters were selected and simulated to calculate the T_{IPM} under each combination, and the results are shown in tab. 5. The temperature distribution is shown in fig. 11.

As can be seen from tab. 5, the T_{IPM} increases then decreases, and finally increases slightly as the thickness of the heat sink plate increases while the sum of the thickness of the heat sink plate and the height of the protruding table remains constant. As mentioned in the previous analysis, the thickness of the heat sink plate and the height of the protruding table have an interactive effect on the T_{IPM}. A change in one of the two parameters will have some effect on the path of heat transfer. The thermal resistance changes with the change in the path of heat exchange, which in turn makes the T_{IPM} change. Figure 11 shows the temperature distribution at different combinations of parameters. Under the combination of fig. 11(b), the T_{IPM} is the highest and the high temperature region is the largest, indicating that the path of heat transfer is the longest and the total thermal resistance is the maximum under this combination of parameters.

Table 5. Simulation results with different combinations of parameters

Parameters		T_{IPM} [K]
t [mm]	h [mm]	
6	4	350.34
7	3	351.04
8	2	349.47
9	1	349.09
10	0	349.18

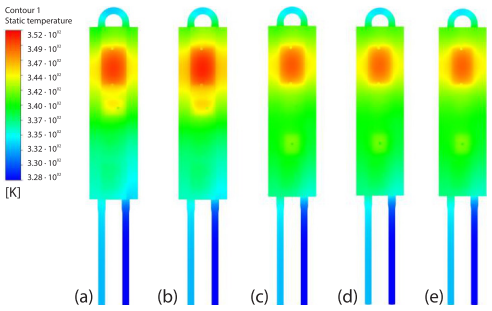

Figure 11. Temperature distribution at different combinations of parameters; (a) 6 + 4 mm, (b) 7 + 3 mm, (c) 8 + 2 mm, (d) 9 + 1 mm, and (e) 10 + 0 mm

Optimization of by Taguchi method

Taguchi method is a robust design optimization method, which uses discrete determination of control factors to achieve the optimal value of the target. The basic idea of Taguchi method is: first determine the factors and their levels, collocate them evenly and establish an appropriate orthogonal test table, and then establish a model according to the parameter combination scheme of the test table to carry out simulation. Then the influence law and the contribution rate of the factors on the responses can be obtained by main effect analysis and extreme difference normalization of the simulation results.

Orthogonal experimental design

In this paper, three parameters were studied with five levels of each factor, as shown in tab. 6.

Table 6. Ranges and levels of parameters

Parameters	A (d [mm])	B (t [mm])	C (h [mm])
Level 1	4	6	0
Level 2	5	7	2
Level 3	6	8	3
Level 4	7	9	4
Level 5	8	10	5

The results of the experimental design are shown in tab. 7, with a total of 25 groups of experimental schemes. In the orthogonal array, the number of occurrences of different numbers in each column is the same, which indicates that it is fair to use the main effect plot to compare the influence of the three factors. The contribution rate of each factor can be defined:

$$\text{Contribution ratio}\left(A\right)=\frac{Y_{\max,A}-Y_{\min,A}}{\sum_{i}^{A,B,C,D}\left(Y_{\max,i}-Y_{\min,i}\right)} \tag{5}$$

Analysis of variance

The results of ANOVA are listed in tab. 8. Where DoF, SS, V, and F-test represent degrees of freedom, sum of squares, variance and value of statistics. The results show that the pipe diameter (A) has the greatest effect on T_{IPM}, followed by B and C. For ΔP, the F-values of B and C are 0, indicating that ΔP is only affected by the pipe diameter (A). It can be learned that the most significant factor affecting both T_{IPM} and ΔP is the pipe diameter. Although the influence of B and C on the pressure drop is not significant, the influence of these two factors on the T_{IPM} cannot be ignored. Therefore, these three parameters must be considered and paid attention in the design and optimization of the heat sink.

Table 7. The orthogonal array and responses

Case No.	Structural parameters			Responses	
	A	B	C	T_{IPM} [K]	ΔP [Pa]
1	4	6	0	345.806	26522.970
2	4	7	2	344.84	26155.110
3	4	8	3	344.39	26648.310
4	4	9	4	344.27	26727.620
5	4	10	5	344.3	26651.990
6	5	6	2	348.26	4206.600
7	5	7	3	346.07	4210.000
8	5	8	4	347.26	4185.910
9	5	9	5	347.04	3710.990
10	5	10	0	346.94	3821.660
11	6	6	3	349.9	962.150
12	6	7	4	348.68	1032.500
13	6	8	5	348.95	963.380
14	6	9	0	348.61	1039.190
15	6	10	2	348.05	1042.100
16	7	6	4	350.34	385.430
17	7	7	5	350.89	359.890
18	7	8	0	350.79	382.790
19	7	9	2	349.52	365.710
20	7	10	3	350.57	363.670
21	8	6	5	351.71	164.390
22	8	7	0	352.76	161.650
23	8	8	2	351.336	162.160
24	8	9	3	351.05	159.480
25	8	10	4	349.87	163.640

Table 8. Analysis of variance for T_{IPM} and ΔP

Factors	DoF	Sum of square		Variance		F-test	
		T_{IPM}	ΔP	T_{IPM}	ΔP	T_{IPM}	ΔP
A	4	140.52	2580545681	35.13	645136420.25	60.70	27118
B	4	4.93	12532	1.23	3133	0.17	0.00
C	4	2.15	87922	0.54	21980	0.07	0.00
Error	20	4.49	375345	0.22	12197334		
Total	32	152.09	2581021480				

Sensitivity analysis of parameters on T_{IPM} and ΔP

Figure 12 shows the sensitivity analysis of parameters to T_{IPM}, in which fig. 12(a) is the main effect plot, and fig. 12(b) is the contribution ratio of different parameters. Analyzed from the perspective of the slope of the main effect plot line, the pipe diameter is positively correlated with the T_{IPM} and the thickness of the heat sink plate is negatively correlated with T_{IPM}, while the T_{IPM} first decreases and then increases as the height of the protruding table increases, which is consistent with the conclusion of the analysis in section *Results and discussions*. Analyzing the response in terms of the mean extreme difference, the pipe diameter contributes the most to the T_{IPM}, and the heat sink's thickness and the protruding table's height make smaller contributions. Figure 12(b) shows quantitatively the comparison of the contribution ratios of different factors on T_{IPM}. The contribution ratios of the three factors are 75.40%, 14.35%, and 10.25% from high to low, respectively. In the optimization, priority should be given to reducing the tube diameter, while slightly increasing the thickness of the heat sink plate and the height of the protruding table, so that it is easier to achieve a lower temperature.

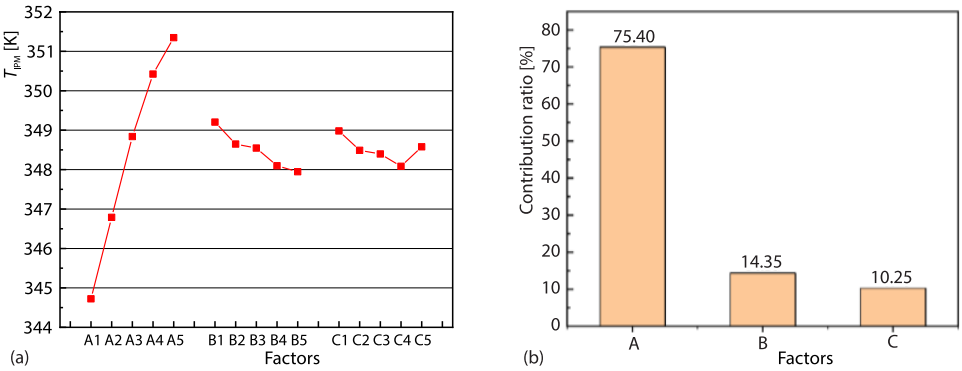

Figure 12. Sensitivity analysis of parameters on T_{IPM}; (a) main-effect plots for T_{IPM} and (b) contribution ratio for T_{IPM}

According to the analysis in the previous section, the change of B and C has no effect on the state of the fluid in the pipe-line. After calculation, the contribution ratio of the pipe diameter reaches 99.18%, while the contribution ratios of B and C are 0.24% and 0.58%, respectively. Therefore, a way of increasing the pipe diameter must be adopted to achieve a lower pressure drop.

Structural optimization and validation

Table 9 shows the settings for multi-objective optimization, including target values, upper and lower limits, contribution ratios and importance. The contribution ratios of all factors and target responses are set to 0.1, and the importance is set to 1.

Table 9. Optimization settings

Name	Goal	Lower limit	Upper limit	Contribution ratio	Importance
A [mm]	Is in range	4	8	0.1	1
B [mm]	Is in range	5	10	0.1	1
C [mm]	Is in range	0	5	0.1	1
T_{IPM} [K]	Minimize	350.184	355.598	0.1	1
ΔP [Pa]	Minimize	141.329	871.094	0.1	1

Table 10 shows the results of the optimization and validation. The best overall performance of the heat sink is obtained for a pipe diameter of 6.77 mm, a heat sink plate thickness of 9.24 mm, and a protruding table height of 5.00 mm. Desirability is 1. Compared to the original structure, there is a slight increase in pressure drop, but the temperature drops by 3.98 K. The verification results show that the deviations between the simulation results and the optimization results of the comprehensive performance of the heat sink are –0.10% and 0.479%, respectively, which is in good agreement.

Table 10. Optimization results and validation

A [mm]	B [mm]	C [mm]		T_{IPM} [K]	ΔP [Pa]
6.77	9.24	5.00	Optimization	346.47	502.36
			CFD simulation	346.11	503.58
			Relative error	0.10%	0.24%

Conclusions

A parametric study of the heat sink for cooling IPM is carried out by the Taguchi method to investigate the effects of key parameters on thermal-hydraulic performance. The main conclusions have been drawn.

- The effects of different structural parameters on the thermal performance and flow characteristics of the heat sink were analyzed.
- As the pipe diameter increases, the T_{IPM} gradually increases, while the pressure drop and entropy generation gradually decrease.
- In the studied range, when the thickness of the heat sink plate increases, the T_{IPM} decreases and then increases, while the entropy generation shows the opposite trend. As the height of the protruding table increases, the T_{IPM} decreases while the entropy generation increases. These two factors have an interactive effect on T_{IPM}. Changes in both affect the path of heat transfer, causing a change in thermal resistance, which in turn affects the T_{IPM}.
- The sensitivity of T_{IPM} and ΔP to different parameters was analyzed. For T_{IPM}, the contribution ratios are from high to low: pipe diameter, the thickness of the heat sink plate, the height of the protruding table. For ΔP, the contribution ratio of pipe diameter reaches 99.18%, while the contribution ratio of the thickness of the heat sink plate and the height of the protruding table is very low.
- The structural parameters of the heat sink were optimized and verified. The optimal combination of parameters was obtained with the objective of minimizing both T_{IPM} and ΔP. Compared with the original structure, there is a slight increase in pressure drop, but T_{IPM} is reduced by 3.98 K.

Nomenclature

c_p – specific heat, [Jkg^{-1}K^{-1}]
$\dot{m}$ – mass-flow rate, [kg^{s-1}]
ΔP – pressure drop, [Pa]
Q – heat load, [W]
s – entropy, [kJkg^{-1}K^{-1}]
T – temperature, [K]
u – velocity, [ms^{-1}]

Greek symbols

λ – thermal conductivity, [WK^{-1}m^{-1}]
μ – viscosity, [Pa·s]
ρ – density, [kgm^{-3}]

Acknowledgment

This work was financially supported by the National Natural Science Foundation of China (No. 52276019), and National Natural Science Foundation of China (No. 52006164).

References

[1] Wang, P., *et al*., Hybrid Solid-And Liquid-Cooling Solution for Isothermalization of Insulated Gate Bipolar Transistor Power Electronic Devices, IEEE Transactions on Components, *Packaging and Manufacturing Technology*, *3* (2012), 4, pp. 601-611
[2] Lostetter, A., *et al.*, An Overview to Integrated Power Module Design for High Power Electronics Packaging, *Microelectronics Reliability*, *40* (2000), 3, pp. 365-379
[3] Choi, U.-M., *et al*., Study and Handling Methods of Power IGBT Module Failures in Power Electronic Converter Systems, *IEEE Transactions on Power Electronics*, *30* (2014), 5, pp. 2517-2533
[4] Yuan, W., *et al*., Numerical Simulation of the Thermal Hydraulic Performance of a Plate Pin Fin Heat Sink, *Applied Thermal Engineering*, *48* (2012), Dec., pp. 81-88
[5] Han, C.-W., Jeong, S.-B., Evaluation of the Thermal Performance with Different Fin Shapes of The Air-Cooled Heat Sink for Power Electronic Applications, *Journal of International Council on Electrical Engineering*, *6* (2016), 1, pp. 17-25
[6] Rao, Z., Wang, S., A Review of Power Battery Thermal Energy Management, *Renewable and Sustainable Energy Reviews*, *15* (2011), 9, pp. 4554-4571
[7] Liu, C.-K., *et al*., Direct Liquid Cooling for IGBT Power Module, *Proceedings*, 9th International Microsystems, Packaging, Assembly and Circuits Technology Conference (IMPACT), Taipei, Taiwan, 2014, pp. 41-44
[8] Seokkan, K., *et al*., A Bioinspired, Low Pressure Drop Liquid Cooling System for High-Power IGBT Modules for EV/HEV Applications, *International Journal of Thermal Sciences*, *161* (2021), 106708
[9] Lu, J., *et al.*, Investigation of a Rectangular Heat Pipe Radiator with Parallel Heat Flow Structure for Cooling High-Power IGBT Modules, *International Journal of Thermal Sciences*, *135* (2019), Jan., pp. 83-93
[10] Pan, M., Study of the Performance of an Integrated Liquid Cooling Heat Sink for High-Power IGBT, *Applied Thermal Engineering*, *190* (2021), 116827
[11] Natarajan, G., Bezama, R., Microjet Cooler with Distributed Returns, *Heat Transfer Engineering*, *28* (2007), 8-9, pp. 779-787
[12] Bhunia, A., Chen, C.-L.. Jet Impingement Cooling of an Inverter Module in the Harsh Environment of a Hybrid Vehicle, *Heat Transfer Summer Conference*, *47349* (2005), Jan., pp. 561-567
[13] Wang, Y., *et al*., Reliability Enhancement by Integrated Liquid Cooling in Power IGBT Modules for Hybrid and Electric Vehicles, *Microelectronics Reliability*, *54* (2014), 9-10, pp. 1911-1915
[14] Yang, P., *et al*., Investigation and Optimization of an Intelligent Power Module Heat Sink Using Response Surface Methodology, *Case Studies in Thermal Engineering*, *28* (2021), 101410
[15] Hu, W., Wei, C., Numerical Simulation and Optimization of Heat Dissipation Structure for High Power Insulated Gate Bipolar Transistor (IGBT), *Journal of Physics: Conference Series*, *2290* (2022), 012122
[16] Cheng, M., *et al*., The Analysis of Numerical Simulation about Thermal Management on Frequency Converter, *IEEE Access*, *7* (2019), Oct., pp. 145677-145684
[17] Deng, Y., Liu, J., Hybrid Liquid Metal-Water Cooling System for Heat Dissipation of High Power Density Microdevices, *Heat and Mass Transfer*, *46* (2010), 11, pp. 1327-1334
[18] Hayashi, Y., *et al*., Thermal Performance and Pressure Drop of Galinstan-Based Micro-Channel Heat-Sink for High Heat-Flux Thermal Management, International Conference on Nanochannels, *Micro-Channels, and Minichannels*, *56871* (2015), V001T07A012
[19] Yerasimou, Y., *et al*., Thermal Management System for Press-Pack IGBT Based on Liquid Metal Coolant, IEEE Transactions on Components, *Packaging and Manufacturing Technology*, *10* (2020), 11, pp. 1849-1860
[20] Wang, P., *et al*., Two-Phase Liquid Cooling for Thermal Management of IGBT Power Electronic Module, *Journal of Electronic Packaging*, *135* (2013), 2, 021001
[21] Gunes, S., *et al*., A Taguchi Approach for Optimization of Design Parameters in a Tube with Coiled Wire Inserts, *Applied Thermal Engineering*, *31* (2011), 14-15, pp. 2568-2577
[22] Yu, C.-L., *et al.*, Parameters Optimization of a Parallel-Flow Heat Exchanger with a New Type of Anti-Vibration Baffle and Coiled Wire Using Taguchi Method, *Journal of Zhejiang University-SCIENCE A*, *19* (2018), 9, pp. 676-690
[23] Yakut, K., *et al*., Experimental Investigation of Thermal Resistance of a Heat Sink with Hexagonal Fins, *Applied Thermal Engineering*, *26* (2006), 17-18, pp. 2262-2271
[24] Yakut, K., *et al*., Optimum Design-Parameters of a Heat Exchanger Having Hexagonal Fins, *Applied Energy*, *83* (2006), 2, pp. 82-98

[25] Wang, H., *et al*., Parametric Study and Optimization of H-Type Finned Tube Heat Exchangers Using Taguchi Method, *Applied Thermal Engineering*, *103* (2016), June, pp. 128-138
[26] Yang, P., *et al*., Investigation and Optimization of Heat Transfer Performance of a Spirally Corrugated Tube Using the Taguchi Method, *International Communications in Heat and Mass Transfer*, *127* (2021), 105577
[27] Zhi, C., *et al*., Numerical Investigation of Slit fin at Different Reynolds Numbers: A Sensitivity Analysis And Optimization by Taguchi Methodology, *International Communications in Heat and Mass Transfer*, *138* (2022), 106393
[28] Du, T., *et al*., Parametric Optimization of Overlapped Helical Baffled Heat Exchangers by Taguchi Method, *Applied Thermal Engineering*, *85* (2015), June, pp. 334-339
[29] Kaluri, R. S., Basak, T., Analysis of Entropy Generation for Distributed Heating in Processing of Materials by Thermal Convection, *International Journal of Heat and Mass Transfer*, *54* (2011), 11

Paper submitted: November 7, 2022
Paper revised: February 3, 2023
Paper accepted: February 6, 2023